Combined use of Landsat-8 and Sentinel-2A images for winter crop mapping and winter wheat yield assessment at regional scale

Sergii Skakun [a,b], Eric Vermote [b], Jean-Claude Roger [a,b], Belen Franch [a,b]

[a] *Department of Geographical Sciences, University of Maryland, College Park, MD 20742, USA*

[b] *NASA Goddard Space Flight Center Code 619, 8800 Greenbelt Road, Greenbelt, MD 20771, USA*

Correspondence author details:

Sergii Skakun

Department of Geographical Sciences, University of Maryland, College Park, MD 20742, USA

NASA Goddard Space Flight Center Code 619, 8800 Greenbelt Road, Greenbelt, MD 20771, USA

Address: NASA GSFC, Code 619, Bldg 32, Room N126-3, Greenbelt, MD 20771, USA

E-mail: skakun@umd.edu; sergii.skakun@nasa.gov

Tel: +1-301-614-5084

Abstract

Timely and accurate information on crop yield is critical to many applications within agriculture monitoring. Thanks to its coverage and temporal resolution, coarse spatial resolution satellite imagery has always been a source of valuable information for yield forecasting and assessment at national and regional scales. With availability of free images acquired by Landsat-8 and Sentinel-2 remote sensing satellites, it becomes possible to enable temporal resolution of an image every 3–5 days, and therefore, to develop next generation agriculture products at higher spatial resolution (30 m). This paper explores the combined use of Landsat-8 and Sentinel-2A for winter crop mapping and winter wheat assessment at regional scale. For the former, we adapt a previously developed approach for Moderate Resolution Imaging Spectroradiometer (MODIS) at 250 m resolution that allows automatic mapping of winter crops taking into account knowledge on crop calendar and without ground truth data. For the latter, we use a generalized winter wheat yield model that is based on NDVI-peak estimation and MODIS data, and further downscaled to be applicable at 30 m resolution. We show that integration of Landsat-8 and Sentinel-2A has a positive impact both for winter crop mapping and winter wheat yield assessment. In particular, the error of winter wheat yield estimates can be reduced up to 1.8 times comparing to the single satellite usage.

Keywords: Landsat-8, Sentinel-2, yield, area, mapping, wheat, MODIS, agriculture, Ukraine

1. Introduction

Timely and accurate information on crop yields at global, national, and regional scales is extremely important for many applications [1]. At national/regional scale, it can be an input to local authorities to make decisions on food security issues or deciding on subsidies in case of extreme weather conditions such as droughts. At field scale, spatial variability of yields can help to obtain objective information, for example, for farmers to improve management practices and identify yield gaps [2], or for insurance companies to feed this information into insurance models [3, 4].

Owing to its coverage, temporal and spatial resolution, remote sensing images from space has always been a powerful tool to develop empirical models for predicting and assessing yields at regional and national scales [5, 6, 7, 8, 9, 10, 11], or assimilating biophysical parameters into crop growth models [12, 13, 14]. In particular, coarse resolution sensors, e.g. Moderate Resolution Imaging Spectroradiometer (MODIS), Advanced Very High Resolution Radiometer (AVHRR), SPOT-VEGETATION, thanks to its daily coverage and availability of historical datasets, have extensively been used for building empirical models for crop yield forecasting and assessment. These models connect satellite-derived features, for example vegetation indices (VIs) such as Normalized Difference Vegetation Index (NDVI), Enhanced Vegetation Index (EVI), Vegetation Health Index (VHI) and/or biophysical parameters such as Leaf Area Index (LAI), Fraction of Photosynthetically Active Radiation (FPAR), with reference yield data. For example, Johnson (2016) [5] analyzed efficiency of multiple MODIS land products including NDVI, EVI, LAI, FPAR, and Gross Primary Production (GPP) to assess crop yield at county level in US for ten major agriculture commodities. He found positive correlations of vegetation products against yield for all crops, except rice, and that finer spatial resolution improved the correlations. López-Lozano et al. (2015) [6] investigated the use of the Fraction of Absorbed Photosynthetically Active Radiation (fAPAR) derived from SPOT-VEGETATION to assess crop yields (wheat, barley and maize) at province level in Europe. They found high correlations (R^2>0.6) in water-stressed regions; however, lower correlations (R^2<0.5) were observed for regions with high yields where water constraints are

less frequent. Salazar et al. (2007) applied AVHRR-derived VHI to estimate winter wheat yield in Kansas, US, and found high correlations with official statistics for 1982–2004 obtaining an error around 8%. In order to overcome some limitations of empirical models in terms of robustness, Becker-Reshef et al. (2010) [10] developed a generalized winter wheat yield forecasting model that was calibrated for one region (US) and successfully applied for another (Ukraine) to provide accuracy of less than 10% that is suitable for operational context. Adding meteorological data, in particular temperature, has usually had a positive effect on crop yield models reducing the error and improving timeliness [5, 6, 7]. Though these models are empirical and based on relative simple equations, they perform at the level or even better than more comprehensive crop growth models that are based on crop growth simulations [8, 15]. The reasons for that are: complexity of accounting multiple factors influencing the yield, lack of high-quality data required to calibrate and run such models, and difficulties of upscaling 'point' estimates to higher spatial scale [16].

Comparing to coarse resolution satellite imagery, the use of Landsat-like (30 m) data to crop yield forecasting and assessment has been limited mainly due to lower temporal resolution. Nevertheless, there were studies aiming at fusing Landsat with MODIS data [17, 18], and combining Landsat with biophysical models [19, 20]. However, these approaches showed mixed results in terms of errors and still had limitations constrained by lower frequency of moderate resolution images. With the combined use of Landsat-8 and Sentinel-2 remote sensing satellites that would enable acquisition of an image every 3–5 days globally, as well as development of cloud platforms such as Google Earth Engine (GEE) [20, 21, 22], it becomes possible to implement approaches similar to those used for MODIS/AVHRR to develop next generation agriculture products at higher spatial resolution (30 m).

This paper presents one of the first studies to combine Landsat-8 and Sentinel-2A imagery for crop yield mapping by downscaling a generalized empirical model developed for MODIS data [7, 10]. The model is based on capturing the peak NDVI to correlate with the yield, and growing degree days (GDD) to improve the timeliness of the model. Therefore, the main objectives of the

study are: (i) to assess performance of downscaling a generalized NDVI-based empirical model for winter wheat yield forecasting from coarse spatial resolution to moderate one at 30 m; (ii) to explore the combined use of images acquired by Landsat-8 and Sentinel-2A remote sensing satellites for winter crop mapping and winter wheat yield assessment at regional level.

2. Study area & materials

2.1. Study area and reference data

The study is performed for Kirohohradska oblast in Ukraine for 2016 (Fig. 1). Oblast is a high-level administrative division of the country (there are 24 oblasts in Ukraine and Autonomous Republic of Crimea), and each oblast is further divided into districts. Kirovhradska oblast is located in the central part of Ukraine and composed of 21 districts with geographical area ranging from 65 to 165 thousand ha and cropland area ranging from 27 to 112 thousand ha. The reasons for selecting this region is that it is a top 10 wheat producer in Ukraine and because of availability of reference crop yield and harvested area data at district scale. Winter wheat is one of the major crops in Kirovhradska oblast accounting for 20% of production of all crops in the region. Winter wheat is mainly rain-fed in the region and usually planted in September-October. After dormancy during the winter, it emerges early spring reaching maturity by the end of June. Harvest of winter crops is typically undertaken in July.

Reference data on crop yield and harvested area at district level were collected from the Department of Agro-Industry Development of Kirovohrad State Administration (http://apk.kr-admin.gov.ua). The data were made available online as the harvest progressed and were based on farm surveys of all large agricultural enterprises (that account of more than 90% of all winter crops production in the region) and samples of household farms the same way as official statistics is collected [23]. The final estimates for winter crop yields and areas were available at the end of November and were used as reference in this study.

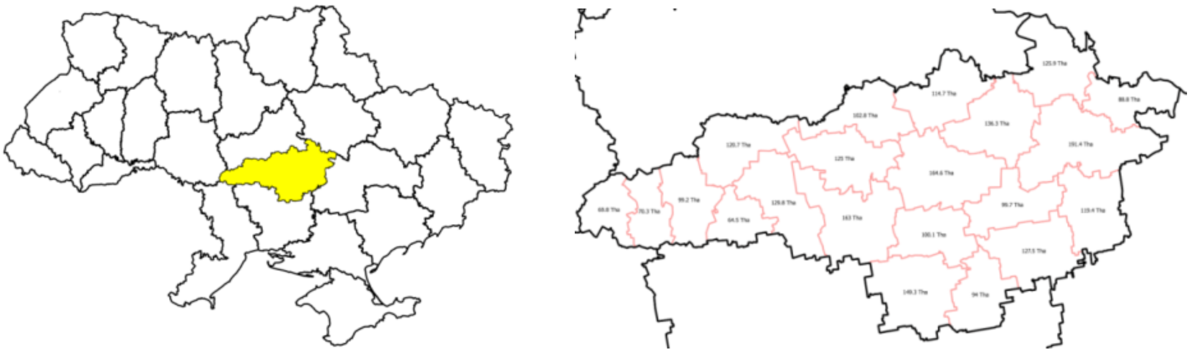

Fig. 1. A map of Ukraine with division into administrative regions (oblasts). The study area (Kirovohradska oblast) is highlighted on *left* figure and shown with division into district on *right* figure.

2.2. Landsat-8/OLI and Sentinel-2A /MSI datasets

Remote sensing images acquired by the Operational Land Imager (OLI) instrument aboard of Landsat-8 satellite and by the Multi-Spectral Instrument (MSI) aboard Sentinel-2A satellite were used in the study. Landsat-8/OLI captures images of the Earth's surface in 9 spectral bands at 30 m spatial resolution (15 m for panchromatic band) [24] while Sentinel-2A/MSI captures images of the Earth's surface in 13 spectral bands at 10 m, 20 m and 60 m spatial resolution [25]. Overall, 51 Landsat-8 and 87 Sentinel-2A scenes were acquired over the study area from March 1, 2016 to July, 31, 2016. Landsat-8 scenes covered the following coordinates (path/row) of the World-wide Reference System (WRS-2): 178/026, 179/026, 179/027, 180/026, 180/027, and 181/026. The swath of the Landsat-8 scene is approximately 185 km × 180 km. Sentinel-2A scenes covered the following tiles: 35UQQ, 35UQP, 36UUV, 36UUU, 36UVV, 36UVU, 36UWV, and 36UWU. The size of the Sentinle-2A tile is approximately 110 km × 110 km.

The Landsat-8/OLI and Sentinel-2A/MSI scenes were atmospherically corrected for surface reflectance using the LaSRC algorithm [26] (Fig. 2) ensuring consistency between these datasets as well as with MODIS data used for building a generalized crop yield model [10, 28]. Cloud and shadow screening for Landsat-8 and Sentinel-2A scenes was performed using the Fmask algorithm [27] and inversion residuals from aerosol optical thickness (AOT) estimation [26] (Fig. 3). The

pixels identified as those with high aerosol content were also masked out. Images from Sentinel-2A/MSI were further converted to 30 m to match spatial resolution of Landsat-8/OLI. Since atmospheric correction for Sentinel-2A was performed at 10 m spatial resolution for all spectral bands, conversion to 30 m was carried out by aggregation (averaging).

It was found that Landsat-8/OLI and Sentinel-2A/MSI exhibit misregistration issues [29]; therefore additional co-registration was performed to ensure spatial consistency between the datasets [30]. Finally, NDVI was calculated for Landsat-8 scenes using band 5 (near-infra red — NIR) and band 4 (red), and for Sentinel-2A scenes using band 8A (NIR) and band 4 (red).

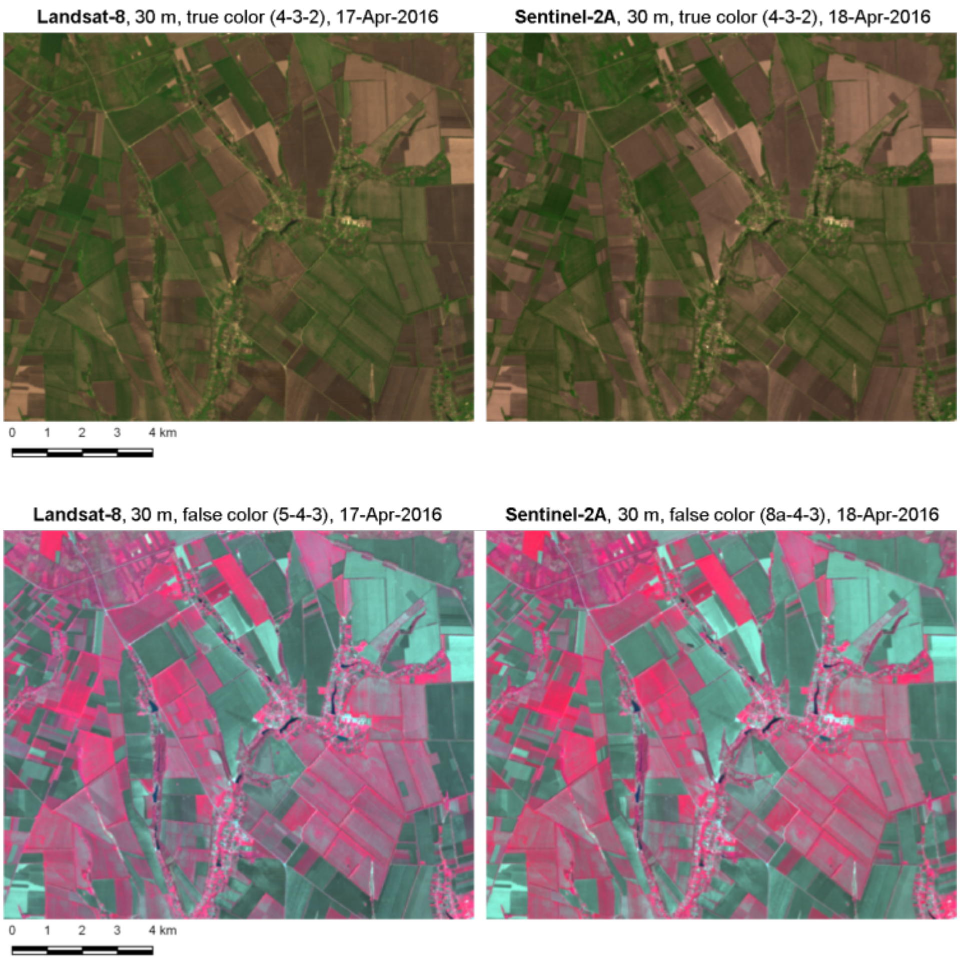

Fig. 2. Examples of images acquired by Landsat-8 and Sentinel-2A satellites 1 day apart and atmospherically corrected using the LaSRC algorithm [26]. True colour images were composed of bands 4-3-2 for Landsat-8 and Sentinel-2A, and scaled from 0 to 0.15. False colour images were composed of bands 5-4-3 for Landsat-8 and 8A-4-3 for Sentinel-2A, and scaled from 0 to 0.3 for NIR, and 0 to 0.1 for red and green bands.

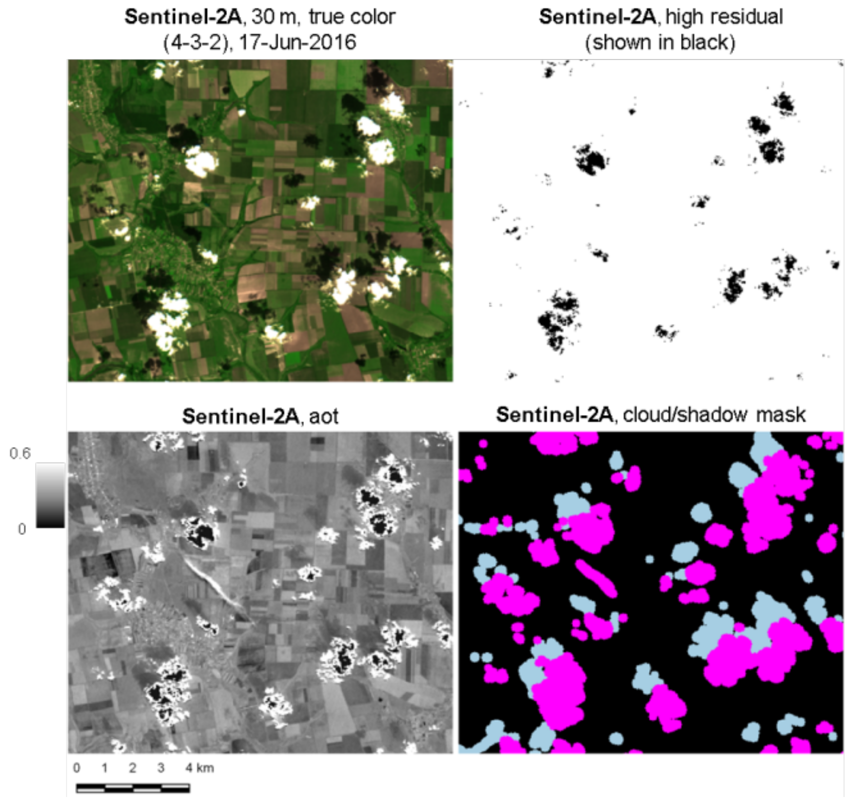

Fig. 3. Example of cloud and shadow detection for Sentinel-2A images

3. Methodology

Winter wheat yield mapping and assessment at regional scale consists of the two major steps: (i) winter crop mapping; (ii) yield assessment at 30 m spatial resolution. Fig. 4 illustrates all processing steps along with input datasets. These steps are described in detail in the following sub-sections.

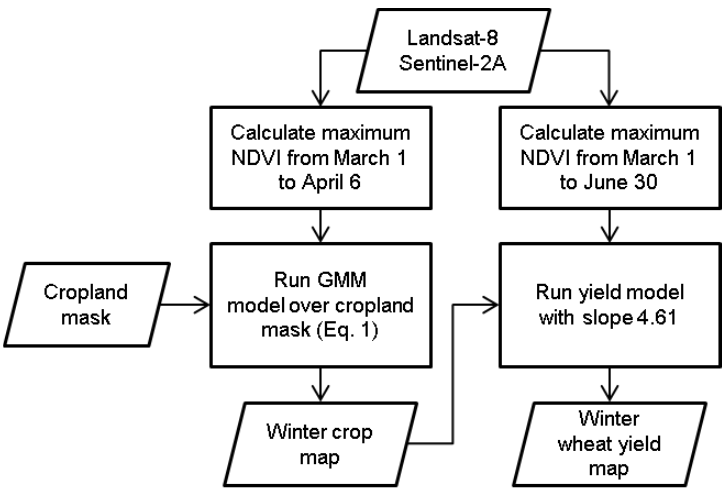

Fig. 4. Algorithm flowchart.

3.1. Winter crop mapping

For winter crop mapping, we adopted a previously developed approach for MODIS [31] that allows automatic mapping of winter crops using a priori knowledge on crop calendar and without using reference (ground truth) data. The method is based on per-pixel estimation of the peak NDVI (metric) during early spring (or early fall depending on hemisphere), when winter crops have developed biomass, while other crops (spring and summer) have no biomass in that time period. The calculated metric will have high NDVI values for winter crops and low NDVI values for other crops (Fig. 5). Then, the metric is modelled using a Gaussian mixture model (GMM) [32] to automatically discriminate different crop types (winter versus others). The GMM is a linear combination of Gaussian distributions that can model any continuous distribution:

$$p(\mathbf{x}) = \sum_{k=1}^{K} \pi_k N(\mathbf{x}|\mu_k, \sum_k), \quad (1)$$

where each Gaussian density $N(\mathbf{x}|\mu_k, \sum_k)$ is called a component of the mixture and has its own mean μ_k and covariance $\sum_k$; parameters π_k are weight (mixing) coefficients with $\sum_{k=1}^{K} \pi_k = 1$ [32].

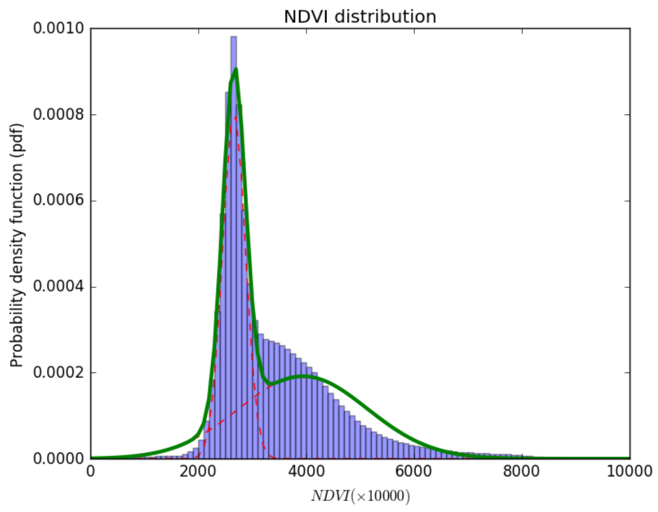

Fig. 5. Empirical distribution for the peak NDVI and fitted GMM model. The solid green line shows the fitted GMM distribution, while the dashed lines show the mixture model components.

Parameters of the GMM model are estimated using an expectation-maximization (EM) algorithm that is run for all pixels identified as cropland. In our study, we used a cropland layer acquired from the land cover map generated for Ukraine at 30 m spatial resolution [33]. The constraint to utilize cropland pixels only comes from potential confusion with grassland, hay, bulrush that might also have already developed biomass within indicated time period. The component with the largest mean in the obtained GMM model is considered to belong to the winter crop class (Fig. 5). Finally, the derived GMM model is applied to all cropland pixels, and a posteriori probability (Eq. 1) of the pixel belonging to the winter crop class is estimated in the final resulting map. Pixels with probability larger than 0.5 are considered as winter crops.

3.2. Winter wheat yield mapping and assessment

Peak NDVI estimated on a per-pixel basis from Landsat-8/OLI and Sentinel-2A/MSI images from March to June was selected as a primary parameter for assessing winter wheat yield. In multiple studies NDVI has been shown to be strongly correlated with yields for a variety of crop types [5, 8, 9, 10]. Since there are no available historical data for a combination of Landsat-8 and Sentinel-2A images to correlate with yield measurements and build a crop yield model at district scale, we used a MODIS-derived winter wheat yield model that was calibrated for US and directly applied for Ukraine [7, 10]. More specifically, the model takes advantage of daily MODIS data at Climate Modeling Grid (CMG) scale at 0.05° resolution to capture an NDVI peak and correlate with the yield. However, since proportion of winter wheat is variable within the CMG pixel, the model establishes a generalized relationship between the slope of NDVI against yield and pixel purity [10]: $s=9.61–0.05*m$, where m is the winter wheat proportion at CMG scale (from 0 to 100%), and s is the slope such as $yield=s*NDVI$.

In case of Landsat-8–Sentinel-2A images, we can assume that purity at 30 m level is 100%, i.e. $m=100$. Therefore, we obtain the slope of 4.61 to be applied to an NDVI peak calculated from the combination of Landsat-8 and Sentinel-2A data to map winter wheat yield at 30 m resolution.

Therefore, the MODIS-derived coarse resolution (0.05°) winter wheat yield model, that was calibrated for US [10], is downscaled using winter wheat purity as a proxy to derive the slope between the peak NDVI and yield. This slope (4.61) is directly applied to the peak NDVI calculated from Landsat-8–Sentinel-2A images to derive a winter wheat yield map at 30 m resolution. These are used to estimate district-level yields by averaging yields at 30 m over winter crop masks (*section 3.1*) for each district. In addition to the average, a standard deviation and coefficient of variation (CV), defined as a ratio between the standard deviation and the mean, is estimated as well. The estimated district-level yields are validated using independent reference data (*section 2.1*) collected at district level in Kirvohradska oblast in Ukraine.

3.3. Validation metrics

For comparison of satellite-derived winter crop areas and winter wheat yield with reference datasets at district level, we used the APU analysis metrics [28]:

- accuracy (*A*) that shows the average bias of the estimates

$$A = \frac{1}{N}\sum_{i=1}^{N}(P_i - O_i), \qquad (2)$$

- precision (*P*) that shows repeatability of the estimates

$$P = \sqrt{\frac{1}{N-1}\sum_{i=1}^{N}(P_i - O_i - A)^2}, \qquad (3)$$

- uncertainty (*U*) that is the root mean squared error

$$U = \sqrt{\frac{1}{N}\sum_{i=1}^{N}(P_i - O_i)^2}, \qquad (4)$$

- relative uncertainty (*rU*) normalized by an average of reference values:

$$rU(\%) = \frac{U}{\frac{1}{N}\sum_{i=1}^{N} O_i}\times 100\% \,, \qquad (5)$$

where P_i and O_i are computed (from satellites) and observed (from reference) values, respectively.

4. Results & discussion

4.1. Winter crop mapping

The GMM approach to winter crop mapping was applied to the peak NDVI calculated for the time period from March 1 to April 6 using a combination of Landsat-8 and Sentinel-2A, as well as using each of them separately. This was done in order to assess an added value of the combined use of these datasets. The indicated period (March 1 to April 6) was selected in such a way to capture NDVI development of winter crops and avoid confusion with early spring cereals that were planted beginning of March. The derived maps were used to calculate the area of winter crops at districts level by pixel-counting. These estimates were compared to reference values and are presented in Table 1 and Fig. 6. The derived winter crop using Landsat-8 and Sentinel-2A is illustrated in Fig. 7.

Table 1. Comparison of satellite-derived winter crop areas with official statistics on harvested areas at district level. Estimates of the *APU* metrics are given in ha.

Metric	LC8-S2A	LC8	S2A
A	612	1081	839
P	1719	5061	1962
U	1785	5056	2090
rU, %	11.6	32.7	13.5
R^2	0.90	0.64	0.88

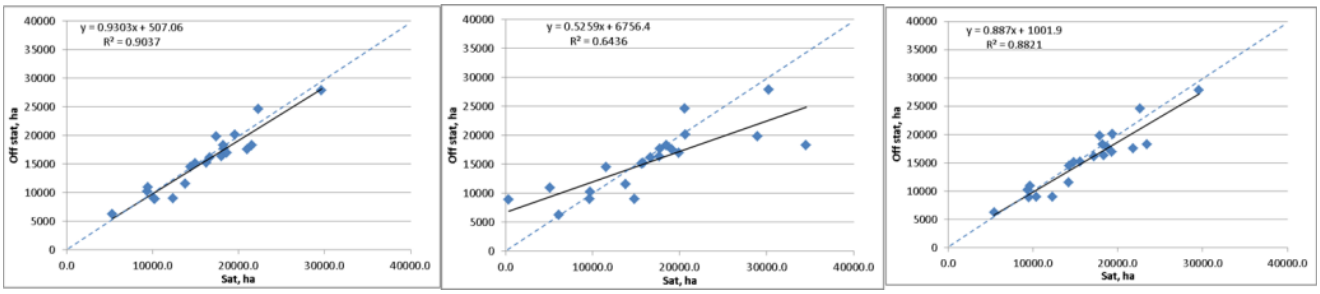

Fig. 6. Plots of official statistics on harvested winter crop areas against satellite-derived ones using a combination of Landsat-8 and Sentinel-2A (*left*), Landsat-8 only (*centre*), and Sentinel-2A only (*right*).

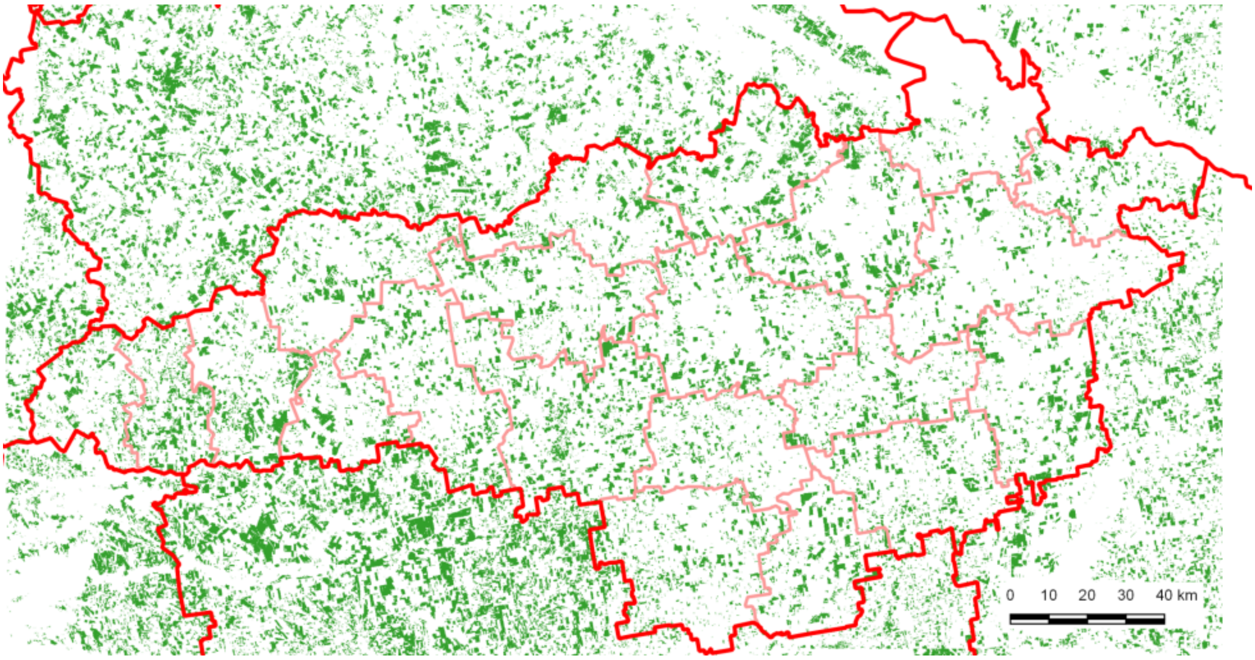

Fig. 7. Final map of winter crops derived from Landsat-8 and Sentinel-2A images using the GMM approach for Kirohradska oblast in 2016.

Combination of Landsat-8 and Sentinel-2A allowed us to achieve $R^2 = 0.9$ and relative uncertainty of 11.6% when estimating winter crop areas at district level. It should be noted that these results were achieved in an automatic way utilizing knowledge on crop calendar and without utilizing any ground truth data. The use of Landsat-8 images only did not produce satisfactory results ($R^2 = 0.64$ and relative uncertainty of 32.7%) because of unavailability of cloud-free images early spring especially in the eastern districts of the oblast whereas the use of Sentinel-2A yielded

$R^2 = 0.88$ and relative uncertainty of 13.5%. Overall, these results demonstrate the benefits, in a quantitative way, of the combined use of Landsat-8 and Sentinel-2A satellites comparing to the single-satellite usage.

4.2. Winter wheat yield mapping

Results of comparison of the estimated winter wheat yields at district level are presented in Table 2 and Fig. 8.

Table 2. Comparison of satellite-derived winter wheat yields with official statistics at district level. Estimates of the *APU* metrics are given in t/ha.

Metric	LC8-S2A	LC8	S2A
A	-0.17	-0.48	-0.34
P	0.26	0.31	0.32
U	0.31	0.57	0.46
rU, %	7.7	14.3	11.5
R^2	0.45	0.29	0.28

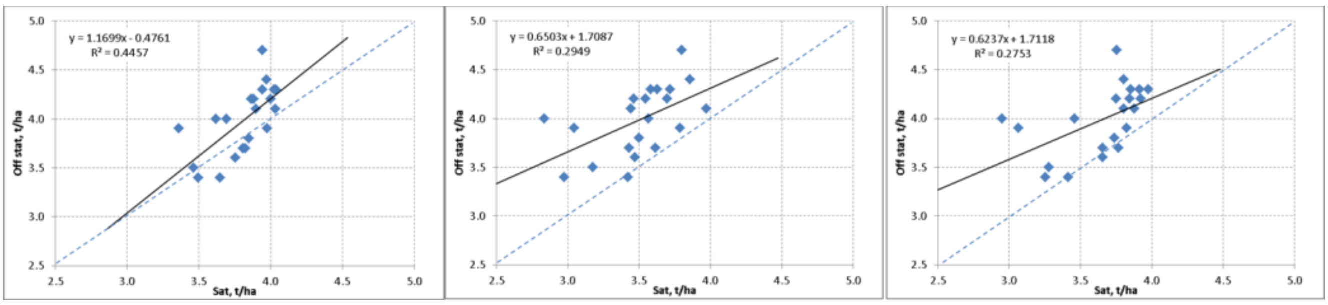

Fig. 8. Plots of official statistics on winter wheat yield against satellite-derived ones using a combination of Landsat-8 and Sentinel-2A (*left*), Landsat-8 only (*centre*), and Sentinel-2A only (*right*).

As with winter crop areas, the combination of Landsat-8 and Sentinel-2A outperformed the single satellite usage. When using either Landsat-8 or Sentinel-2A, the peak NDVI approach underestimated official statistics by -0.48 t/ha and -0.34 t/ha, respectively, while their combination improved to -0.17 t/ha. In terms of uncertainty, the peak NDVI approach for the Landsat-8–Sentinel-2A combination provided 0.31 t/ha (7.7%) whereas those values were 1.8 times higher for the Landsat-8 usage only (0.57 t/ha, 14.3%) and 1.5 times higher for the Sentinel-2A usage only (0.46 t/ha, 11.5%). These results clearly demonstrate the importance of higher observation frequency achieved with combination of Landsat-8 and Sentinel-2A satellites comparing to the single use.

The results presented in Fig. 8 (left) were further analyzed for errors. Overall, the points can be divided into 3 groups. The first group is composed of 3 points representing districts with official statistics yields values close to 4 t/ha and underestimated by the peak NDVI approach. These districts feature relatively large values of CV of 21% whereas the average CV for all other districts is approximately 13%. The reason for that is smaller number of images available for these districts (mainly in the eastern part) which reduces ability to capture the peak NDVI. The second group is composed of districts with official statistics yields larger than 4 t/ha. The reason for that is saturation of NDVI occurs and the proposed approach fails to discriminate yield values at this level. Fig. 9 shows an example of NDVI time-series for the district with reference yield of 4.3 t/ha and estimated yield of 4.04±0.40 t/ha with NDVI quickly achieving the value of 0.8 on April 29 (day of the year (DOY) 120) and not changing considerably (within 0.8–0.9) during the following days 50 days (until June 18 or DOY=170). The NDVI values start to decrease when the senescence phase occurs and the crop is eventually harvested.

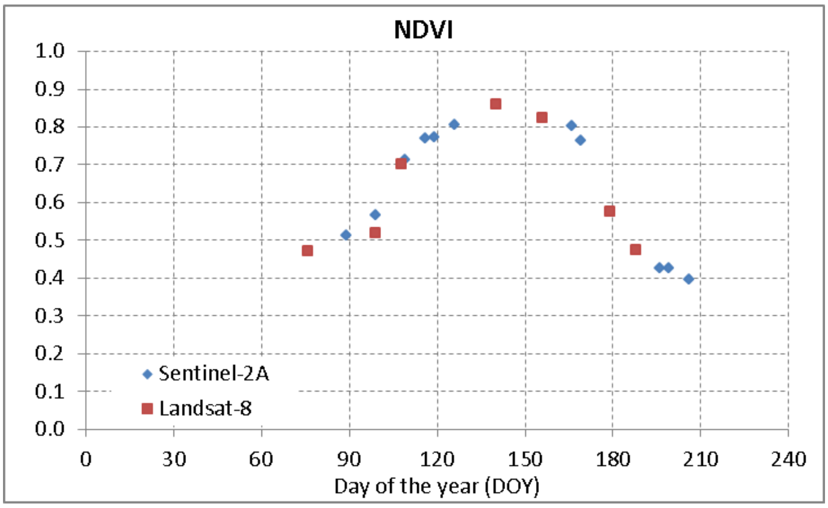

Fig. 9. A combined Landsat-8–Sentinel-2A derived NDVI time-series of winter wheat for the district with reference yield at 4.3 t/ha.

The third group involves 8 districts with moderate yield values of up to 4 t/ha. The proposed approach is able to explain variations in the winter wheat yield (R^2=0.8) giving a bias of 0.1 t/ha and uncertainty of U=0.13 t/ha (3.5%).

6. Conclusion

This study attempted to explore the combined use of Landsat-8 and Sentinel-2A satellites to winter crop mapping and winter wheat yield assessment at regional level. For both tasks, the increased frequency of observations from the satellites was critical as it allowed us to achieve better performance comparing to the single satellite usage. For winter crop mapping, we adopted a previously developed approach for MODIS that allowed automatic winter crop mapping taking into account a priori knowledge on crop calendar without utilizing ground reference data. When comparing to official statistics on winter crop harvested areas, this approach gave R^2=0.9 and relative error of 11.6%. These results are encouraging as with little data inputs (crop calendar and cropland mask) and high temporal resolution of Landsat-8–Sentinel-2A satellites, it would allow the creation of winter crop maps at global scale at 30 m resolution.

For winter wheat yield mapping, we downscaled the generalized empirical model that is based on peak NDVI and was developed using MODIS data, and directly applied it to the Landsat-8–Sentinel-2A images. The model was efficient in explaining moderate yield values (<4 t/ha) with R^2=0.8; however, it failed to capture the variance of high yield values (>4 t/ha) due to NDVI saturation. Overall, the downscaled peak NDVI approach with combined use of Landsat-8 and Sentinel-2A gave uncertainty of 0.31 t/ha (7.7%) and R^2=0.45 substantially outperforming Landsat-8 only (1.8 times) and Sentinel-2A only (1.5 times).

References

1. Becker-Reshef I, Justice C, Sullivan M, et al. (2010) Monitoring global croplands with coarse resolution earth observations: The Global Agriculture Monitoring (GLAM) project. *Remote Sensing* 2(6): 1589–1609.

2. Lobell DB (2013) The use of satellite data for crop yield gap analysis. *Field Crops Research* 143: 56–64.

3. Bokusheva R, Kogan F, Vitkovskaya I, et al. (2016) Satellite-based vegetation health indices as a criteria for insuring against drought-related yield losses. *Agricultural and Forest Meteorology* 220: 200–206.

4. Skakun S, Kussul N, Shelestov A, et al. (2010) The use of satellite data for agriculture drought risk quantification in Ukraine. *Geomatics, Natural Hazards and Risk* 7(3): 901–917.

5. Johnson DM (2016) A comprehensive assessment of the correlations between field crop yields and commonly used MODIS products. *International Journal of Applied Earth Observation and Geoinformation* 52: 65–81.

6. López-Lozano R, Duveiller G, Seguini L, et al. (2015) Towards regional grain yield forecasting with 1 km-resolution EO biophysical products: strengths and limitations at pan-European level. *Agric Forest Meteorol* 206: 12–32.

7. Franch B, Vermote EF, Becker-Reshef I, et al. (2015) Improving the timeliness of winter wheat production forecast in the United States of America, Ukraine and China using MODIS data and NCAR Growing Degree Day information. *Remote Sensing of Environment* 161: 131–148.

8. Kogan F, Kussul N, Adamenko T, et al. (2013) Winter wheat yield forecasting in Ukraine based on Earth observation, meteorological data and biophysical models. *International Journal of Applied Earth Observation and Geoinformation* 23: 192–203.

9. Mkhabela MS, Bullock P, Raj S, et al. (2011) Crop yield forecasting on the Canadian Prairies using MODIS NDVI data. *Agricultural and Forest Meteorology* 151(3): 385–393.

10. Becker-Reshef I, Vermote E, Lindeman M, et al. (2010). A generalized regression-based model for forecasting winter wheat yields in Kansas and Ukraine using MODIS data. *Remote Sensing of Environment* 114(6): 1312–1323.

11. Salazar L, Kogan F, Roytman L (2007) Use of remote sensing data for estimation of winter wheat yield in the United States. *International Journal of Remote Sensing* 28: 3795–3811.

12. Huang J, Sedano F, Huang Y, et al. (2016) Assimilating a synthetic Kalman filter leaf area index series into the WOFOST model to improve regional winter wheat yield estimation. *Agricultural and Forest Meteorology* 216: 188–202.

13. Huang J, Tian L, Liang S, et al. (2015) Improving winter wheat yield estimation by assimilation of the leaf area index from Landsat TM and MODIS data into the WOFOST model. *Agricultural and Forest Meteorology*, *204*, pp.106-121.

14. de Wit A, Duveiller G, Defourny P (2012) Estimating regional winter wheat yield with WOFOST through the assimilation of green area index retrieved from MODIS observations. *Agricultural and Forest Meteorology* 164: 39–52.

15. Kowalik W, Dabrowska-Zielinska K, Meroni M, et al. (2014) Yield estimation using SPOT-VEGETATION products: A case study of wheat in European countries. *International Journal of Applied Earth Observation and Geoinformation* 32: 228–239.

16. Morell FJ, Yang HS, Cassman KG, et al. (2016) Can crop simulation models be used to predict local to regional maize yields and total production in the US Corn Belt? *Field Crops Research* 192: 1–12.
17. Gao F, Anderson MC, Zhang X, et al. (2017) Toward mapping crop progress at field scales through fusion of Landsat and MODIS imagery. *Remote Sensing of Environment* 188: 9–25.
18. Doraiswamy PC, Hatfield JL, Jackson TJ, et al. (2004) Crop condition and yield simulations using Landsat and MODIS. *Remote Sensing of Environment* 92(4): 548–559.
19. Baez-Gonzalez AD, Chen PY, Tiscareno-Lopez M, et al. (2002) Using satellite and field data with crop growth modeling to monitor and estimate corn yield in Mexico. *Crop Science* 42(6): 1943–1949.
20. Lobell DB, Thau D, Seifert C, et al. (2015) A scalable satellite-based crop yield mapper. *Remote Sensing of Environment*, *164*, pp.324-333.
21. Hansen MC, Potapov PV, Moore R, et al. (2013) High-resolution global maps of 21st-century forest cover change. *Science* 342(6160): 850–853.
22. Shelestov A, Lavreniuk M, Kussul N, et al. (2017) Exploring Google Earth Engine Platform for Big Data Processing: Classification of Multi-Temporal Satellite Imagery for Crop Mapping. *Front Earth Sci* 5:17. doi:10.3389/feart.2017.00017.
23. Gallego FJ, Kussul N, Skakun S, et al. (2014) Efficiency assessment of using satellite data for crop area estimation in Ukraine. *International Journal of Applied Earth Observation and Geoinformation* 29: 22–30.
24. Roy DP, Wulder MA, Loveland TR, et al. (2014) Landsat-8: Science and product vision for terrestrial global change research. *Remote Sensing of Environment* 145: 154–172.
25. Drusch M, Del Bello U, Carlier S, et al. (2012) Sentinel-2: ESA's optical high-resolution mission for GMES operational services. *Remote Sensing of Environment* 120: 25–36.
26. Vermote E, Justice C, Claverie M, et al. (2016) Preliminary analysis of the performance of the Landsat 8/OLI land surface reflectance product. *Remote Sensing of Environment* 185: 46–56.

27. Zhu Z, Wang S, Woodcock CE (2015) Improvement and expansion of the Fmask algorithm: cloud, cloud shadow, and snow detection for Landsats 4–7, 8, and Sentinel 2 images. *Remote Sensing of Environment* 159: 269–277.

28. Vermote EF, Kotchenova S (2008). Atmospheric correction for the monitoring of land surfaces. *Journal of Geophysical Research: Atmospheres* 113: D23.

29. Storey J, Roy DP, Masek J, et al. (2016) A note on the temporary misregistration of Landsat-8 Operational Land Imager (OLI) and Sentinel-2 Multi Spectral Instrument (MSI) imagery. *Remote Sensing of Environment* 186: 121–122.

30. Skakun S, Roger JC, Vermote E, et al. (2017) Automatic sub-pixel co-registration of Landsat-8 Operational Land Imager and Sentinel-2A Multi-Spectral Instrument images using phase correlation and machine learning based mapping. *International Journal of Digital Earth*, doi: 10.1080/17538947.2017.1304586, in press.

31. Skakun S, Franch B, Vermote E, et al. (2017). Early season large-area winter crop mapping using MODIS NDVI data and growing degree days information. *Remote Sensing of Environment* (under revision).

32. Bishop CM (2006) *Pattern Recognition and Machine Learning*. New York: Springer.

33. Lavreniuk M, Kussul N, Skakun S, et al. (2015) Regional retrospective high resolution land cover for Ukraine: Methodology and results. In: *2015 IEEE International Geoscience and Remote Sensing Symposium, IGARSS2015,* New York: IEEE, 3965–3968.